Diversified physiological sensory input connectivity questions the existence of distinct classes of spinal interneurons in the adult cat in vivo

Matthias Kohler[a,1,*], Fredrik Bengtsson[b,1], Philipp Stratmann[a,c], Florian Röhrbein[a], Alois Knoll[a], Alin Albu-Schäffer[a,c], Henrik Jörntell[b]

[a] *Technical University of Munich, Department of Informatics, Garching, 85748, Germany*
[b] *Lund University, Department of Experimental Medical Science, Lund, 22184, Sweden*
[c] *German Aerospace Center, Institute of Robotics and Mechatronics, Weßling, 82234, Germany*

Abstract

The spinal cord is engaged in all forms of motor performance but its functions are far from understood. Because network connectivity defines function, we explored the connectivity for muscular, tendon and tactile sensory inputs among a wide population of spinal interneurons in the lower cervical segments. Using low noise intracellular whole cell recordings in the decerebrated, non-anesthetized cat in vivo, we could define mono-, di-, trisynaptic inputs as well as the weights of each input. Whereas each neuron had a highly specific input, and each indirect input could moreover be explained by inputs in other recorded neurons, we unexpectedly also found the input connectivity of the spinal interneuron population to form a continuum. Our data hence contrasts with the currently widespread notion of distinct classes of interneurons. We argue that this more diversified physiological connectivity, which likely requires a major component of circuitry learning, implies a more flexible functionality.

1. Summary

2. Introduction

The spinal cord contains a potentially highly complex but poorly understood neuronal circuitry. Because of its position, it is pivotal to any aspect of brain action that involves movement (Crone et al., 2008; Bui et al., 2013; Azim et al., 2014) and its potential contributions to brain function can be considered underestimated (Loeb and Tsianos, 2015). In addition, because of the tight linkage between cognitive development and the development of movement (Diamond, 2000; Chiaravalloti et al., 2020), the functional principles of the spinal cord circuitry are potentially fundamental to many higher order functions by virtue of impacting how the brain perceives the world (Rongala et al., 2018).

The spinal cord has motoneurons, which connect to the muscles, and interneurons, which are all spinal neurons that are not motoneurons. A very early identified type of interneuron are the Renshaw cells, which get input from motoneurons and inhibit motoneurons (Eccles et al., 1954). Next the Ia-inhibitory-interneuron was identified as neurons receiving input from the Ia afferent and inhibiting motoneurons and other Ia-inhibitory-interneurons (Hultborn et al., 1971). Subsequent research focused on identifying more types of neurons, by their input, how the input arrived at the neuron, their location and synaptic action (Reviewed by Jankowska (1992) and McCrea (1992)). The types of neuron considered so far however are not distinct, and some types clearly share features with other types (Jankowska and Edgley, 2010; Hultborn, 2001). Though we are not aware of a publication that explicitly describes a classification scheme, that assigns all spinal neurons into disjoint classes, this type of attempted neurophysiological classification approach had the aim of identifying all the specific interneuron types that existed McCrea (1992), with the implied goal that eventually the resulting gigantic network puzzle was going to be solvable. More recently, spinal interneuron types were also found to be separable on basis of their patterns of gene expression, which are present in early development (Jessell, 2000; Goulding, 2009). More than forty different subtypes of spinal interneurons have been identified on basis of differences in gene expression (Gabitto et al., 2016). Recent studies suggested that the patterns of synaptic connectivity, or network formation, could be based on genetic preprogramming, where chemoattractants emitted by one interneuron type would attract synaptic inputs from a specific input source or specific other interneuron types, creating the vision that the neurophysiological and genetic classification schemes could be mapped to each other (Chen et al., 2006; Pecho-Vrieseling et al., 2009; Bikoff, 2019). Here we investigated the

*Corresponding author
Email addresses: kohler@in.tum.de (Matthias Kohler), fredrik.bengtsson@med.lu.se (Fredrik Bengtsson), Philipp.Stratmann@dlr.de (Philipp Stratmann), florian.roehrbein@in.tum.de (Florian Röhrbein), knoll@in.tum.de (Alois Knoll), Alin.Albu-Schaeffer@dlr.de (Alin Albu-Schäffer), henrik.jorntell@med.lu.se (Henrik Jörntell)
[1] These authors contributed equally to this work.

input connectivity of spinal interneurons throughout the lower cervical spinal cord using intracellular recordings to define the synaptic linkage of their excitatory and inhibitory synaptic inputs from a set of peripheral input sources in vivo. Our findings suggest an absence of distinct rules of connectivity, which would argue for that the connectivity of the spinal cord circuitry in adult mammals to a large extent could be defined by learning.

3. Methods

3.1. Resource availability

Lead contact

Further information and requests for resources should be directed to and will be fulfilled by the lead contact, Matthias Kohler `kohler@in.tum.de`.

Materials availability

This study did not generate new unique reagents.

Data and code availability

Clustering algorithms are implemented in R using the `cluster` (Maechler et al., 2019) and the `sigclust` packages. Swap randomization, association rule and graph structure analysis are implemented in custom C++ software. The data and code will be made available upon publication at Zenodo.

3.2. Experimental model and subject details

The procedures of all experiments were approved in advance by the local Swedish Animal Research Ethics Committee (permits M32-09 and M05-12). Adult cats were prepared as previously described (Jörntell and Ekerot, 2002, 2006; Spanne et al., 2014). Briefly, following an initial anesthesia with propofol (Diprivan^{TM}Zeneca Ltd, Macclesfield Cheshire, UK), the animals were decerebrated at the intercollicular level and the anesthesia was discontinued. The animals were artificially ventilated and the end-expiratory CO_2, blood pressure and rectal temperature were continuously monitored and maintained within physiological limits. Mounting in a stereotaxic frame, drainage of cerebrospinal fluid, pneumothorax and clamping the spinal processes of a few cervical and lumbar vertebral bodies served to increase the mechanical stability of the preparation. To verify that the animals were decerebrated, we made EEG recordings using a silver ball electrode placed on the surface of the superior parietal cortex. Our EEG recordings were characterized by a background of periodic 1 kHz to 4 kHz oscillatory activity, periodically interrupted by large-amplitude 7 kHz to 14 kHz spindle oscillations lasting for 0.5 s or more. These forms of EEG activities are normally associated with deep stages of sleep (Niedermayer and Lopes Da Silva, 1993). The pattern of EEG activity and the blood pressure remained stable, also on noxious stimulation, throughout experiments (see also (Jörntell and Ekerot, 2006)). Laminectomies were performed from spinal segments C3 to T1. Clamps were put on vertebra T1 and around vertebrae L1-L3. The dura was cut and a local, stabilizing coil of Teflon-coated silver wire was put on the surface of the recording area. We also made small openings in the pia mater in order to facilitate penetration of the patch clamp pipettes. The recording region was covered with agarose attached to the bone of the vertebrae in order to dampen tissue movements. See Figure 1 A for an illustration of the general experimental setup.

3.3. Method details

3.3.1. Stimulations

In order to study synaptic integration in the recorded neurons, we used a set of input sources which were electrically stimulated to evoke synaptic inputs to the recorded neurons. These consisted of the deep radial (DR) nerve, for the activation of muscle afferent inputs of type Ia and of type Ib (corresponding to muscle spindle afferents and Golgi tendon organ afferents, respectively), and the skin area that by manual identification could be identified as the most sensitive for that specific neuron. The DR nerve does not contain any skin afferents but supplies the Extensor carpi radialis brevis, Supinator, Posterior interosseous nerve (a continuation of the deep branch after the supinator), Extensor digitorum, Extensor digiti minimi, Extensor carpi ulnaris, Abductor pollicis longus, Extensor pollicis brevis, Extensor pollicis longus and the Extensor indicis. A bipolar stimulation electrode was mounted around the DR nerve, which was dissected to gain access to wrap the stimulation electrode around it but otherwise leaving the DR nerve intact. The nerve and the stimulation electrodes were embedded in cotton drenched in paraffin oil to prevent spread of stimulation current into the surrounding tissue. In order to activate input from the identified skin receptive field of the neuron, we also inserted a pair of bipolar skin stimulation needle electrodes (separated by about 5 mm to 7 mm) into the epidermis and used single pulse electrical bipolar stimulation of maximum 2 mA, 0.14 ms pulse width, which activates only tactile cutaneous receptors (Bengtsson et al., 2013).

3.3.2. Obtaining recordings

Patch clamp pipette electrodes were pulled to impedances of 4 MΩ to 14 MΩ (Jörntell and Ekerot, 2006; Spanne et al., 2014). The pipettes were back-filled with an electrolyte solution containing potassium gluconate (135 mM), HEPES (10 mM), KCl (6.0 mM), Mg-ATP (2 mM), EGTA (10 mM). The solution was titrated to 7.35–7.40 using 1 M KOH. The recording electrodes were inserted vertically through the dorsal surface of the exposed spinal cord and spinal neurons were recorded from the lower cervical segments (C6-C8) at depths of 1.3 mm to 3.9 mm, corresponding to laminae III-VIII (Figure 1 B) (Rexed, 1952). Since all but two of the recordings were made above the depth of the alpha-motoneurons they were from putative spinal interneurons. The recording signal was converted to a digital signal using the analog-to-digital converter Power 1401 mkII from Cambridge Electronic Design (CED, Cambridge, UK). The neural recordings were continuous and sampled at 100 kHz with the software Spike 2 from CED. In order to facilitate the analysis of evoked excitatory postsynaptic potentials (EPSPs) and inhibitory postsynaptic potentials (IPSPs), a mild (10-30 pA) hyperpolarizing bias current was injected through the recording electrode to suppress spiking activity. Before and after the neuron was recorded intracellularly, we also recorded extracellularly to allow a field potential analysis of the inputs evoked by the sensory stimulations.

We recorded from 114 spinal interneurons, with 68 spinal interneuron recordings in the whole cell mode, where the recording quality allowed the identification of the amplitude of individual synaptic responses, and thus permitted a synaptic weight analysis (Figure 2). The remainder of the recordings ($n = 46$) were not fully under whole cell control but still partially intracellular and were hence used as additional material used in the analysis of the input connectivity of the peripheral inputs to the spinal interneurons.

3.3.3. Analysis of PSPs

To identify a threshold stimulation intensity for each response component, each input was activated at a number of different intensities, with a high number of repetitions for each intensity. All responses were analyzed using a custom-made software, which allowed a template-based identification of EPSPs and IPSPs (Figures 1 D and 2 A). These templates were created from spontaneous unitary EPSPs or spontaneous IPSPs, which were also congruent with unitary PSPs evoked at low-threshold stimulation of peripheral afferents. Evoked responses were analyzed using fitting of the template PSP shapes through scaling. The analysis aimed to define the input connectivity to each neuron. This means whether the input was mono-, di- or trisynaptic, in addition to whether it was excitatory or inhibitory.

Two types of field potentials were used to determine PSP latency. First, the afferent fiber **volley**, which is the field potential evoked by action potentials from the afferents entering the spinal cord. Second, the synaptic local field potential (**LFP**) which is caused by synaptic currents evoked by the afferent fiber volley.

Also the respective minimal threshold intensities for evoking a response were identified in this way. Response latency times were analyzed as the relative time to these field potential latency times, which made the identification of monosynaptic responses straight forward (Figure 2 D,F) (Quevedo et al., 2000; McCrea et al., 1995). In addition, monosynaptic responses could be separated from non-monosynaptic responses by their lower variability in response latency time and peak amplitude. Di-synaptic responses could be identified by their relatively minor difference of the response latency time compared to the monosynaptic response. Trisynaptic responses were separable from di-synaptic responses again in part on the differences in response latency times and relative latency to a di-synaptic response. The analysis of indirect PSP responses that were preceded by earlier PSP response components was supported by the identification of the template shapes of the EPSPs and IPSPs of each neuron. In particular, indications of rapid changes in the membrane potential that were incompatible with the expected decay phase of the template PSPs, and which was followed by the apparent addition of a new PSP component, based on template-shape identification, was taken as an indication of an another evoked PSP with a longer synaptic linkage.

3.3.4. Statistics

Classes of Spinal Interneurons. We used statistical tests and machine learning algorithms to determine if the spinal interneurons fell into well separated classes and to find patterns indicative of any formative process that could explain the input connectivity to the neurons. These tests did not assume a priori that a subdivision or any specific pattern must exist, hence allowing an unbiased evaluation of the input connectivity to the spinal interneurons.

In order to determine if an input-based subdivision of the neurons existed we used two conceptually similar but separate tests. The first method, SigClust(Liu et al., 2008) tests the hypothesis that the data comes from a single Gaussian distribution (Figure 5B). To achieve this, the clusterability of the actual dataset is compared to that of data generated by sampling ($n = 10000$) from a Gaussian distribution. The Gaussian distribution was constructed by fitting it to the data, so that the mean and the variance were identical to that of the recorded data. The cost of a clustering, also called clusterability, is defined

as the sum of the distances of the data points to the mean of the clusters. The cluster index is the fraction between the cost of clustering the data into two cluster and into one cluster. The cluster indices of the generated data are computed, giving a distribution of cluster indices. If the clustering index of the original dataset falls into the 0.05 quantil of the distribution then the hypothesis can be rejected and the actual dataset is determined to be clusterable into at least two clusters. This method is suitable for high dimensional, low sample size data and has been applied previously in the context of biological data analysis (Liu et al., 2008; Verhaak et al., 2010; Burstein et al., 2015; Prat et al., 2010).
The second method, GapStatistics(Tibshirani et al., 2001), is conceptually similar to the SigClust method. It compares the actual data to a random distribution (Figure 5D). Additionally, the GapStatistics determines the correct number of clusters. A possible outcome is that the number of clusters is estimated to be only one cluster or that there is as many clusters as there are datapoints. In both these cases the dataset is considered unclusterable. The GapStatistics measures how far the clustering cost of the dataset differs from the clustering cost of the reference random distribution (a uniform distribution fitted to the actual dataset) for any given number of clusters. To achieve this, random samples ($n = 2000$) are drawn from the reference distribution, and their average clustering cost is computed. Then the original data is clustered and the clustering cost is computed. The gap is the difference between the logarithmic value of the clustering cost of the actual dataset and the logarithmic value of the average clustering cost of the random samples. The number of clusters is estimated as the number which maximises the gap. This method has also been applied to analyse biological data (Tothill et al., 2008; Grün et al., 2015; Viventi et al., 2011).

Associations between neuronal inputs. In order to find patterns of input connectivity we used Association Rule Mining (Agrawal et al., 1993). This method finds associations between binary properties in a given dataset. In the present context a binary property is the presence or absence of a specific input connectivity to a spinal interneuron. A potential association of two input connectivities is encoded as a so called association rule $P_1 \Rightarrow P_2$, where P_1 and P_2 are two connectivities from afferents to neurons. Such a rule is to be read as that if a neuron has connectivity P_1 then it also has connectivity P_2. If a neuron has connectivity P_1 then the rule applies to the neuron. If a neuron has connectivity P_1 and connectivity P_2 then the rules applies to the neuron and holds true. If the neuron has connectivity P_1 but does not have connectivity P_2, then the rule applies to the neuron, but does not hold true.
For example, connectivity P_1 is a monosynaptic Ia afferent input, and P_2 an inhibitory disynaptic Ib afferent input. Consider four different imaginary neurons and the rule $P_1 \Rightarrow P_2$. Neuron one has a monosynaptic Ia afferent input and an inhibitory disynaptic Ib afferent input. Neuron two does not have Ia input but does have Ib inhibitory input. Neuron three has the Ia input but not the Ib input. Neuron four has neither input. The rule applies to neuron one and three, but does no apply to neuron two and four. The rule holds true for neuron one and does not hold true for neuron three.
For a set of neurons S the support of the rule $P_1 \Rightarrow P_2$ is

$$supp(P_1 \Rightarrow P_2) = \frac{|\{n \in S \mid \text{Neuron n has connectivity } P_1\}|}{|S|} \quad .$$

The support is the fraction of neurons where the rule applies.
The confidence of a rule

$$conf(P_1 \Rightarrow P_2) = \frac{|\{n \in S \mid \text{Neuron n has connectivity } P_1 \text{ and } P_2\}|}{|\{n \in S \mid \text{Neuron n has connectivity } P_1\}|} \quad ,$$

is the fraction between the number of neurons where the rule applies and where the rule holds true.

Graph structure analysis. We also designed a data analysis method to gain insight into the spinal interneuron network structure. Each neuron gives a glimpse of a fraction of the network connectivity. Our method works by searching for neurons whose input connectivity allows for possible connections between them. Each neuron is characterized by its input connectivity which is a subset of all possible input connections $A = \{\text{Ia}, \text{Ib}, \text{Skin}\} \times \{-4, \ldots, -1, 1, \ldots 4\}$. Here the inputs a neuron receives are encoded as a tuple consisting of the afferent where the input comes from and the number of synapses over which the input is transmitted. Inputs over more than four synapses are ignored. Inhibition is encoded as a negative number.
If a neuron $N' \subseteq A$ gives excitation via n consecutive synaptic linkages to a neuron N, then neuron N receives the following set of excitatory inputs

$$\alpha^n(N') := \{(m, l+n) \mid (m, l) \in N', l > 0, l+n \leq 4\} \subseteq N$$

If a neuron $N' \subseteq A$ gives inhibition via n synapses to a neuron N, then neuron N receives the following set of inhibitory inputs

$$\alpha^{-n}(N') := \{(m, -(l+n)) \mid (m, l) \in N', l > 0, l+n \leq 4\} \subseteq N$$

In both cases neuron N' receives all excitatory input connections that N receives over n more synapses and in the case that N inhibits N', N' receives the input connection as inhibition.
In a network where two neurons $N_1, N_2 \subseteq A$ are connected to each other, the following facts hold.

- If N_1 and N_2 are connected to each other with excitatory synapses, then $\alpha^{+1}(N_1) \subseteq N_2$ and $\alpha^{+1}(N_2) \subseteq N_1$.
- If N_1 is connected to N_2 with an excitatory synapse and N_2 is connected to N_1 with an inhibitory synapse then $\alpha^{-1}(N_1) \subseteq N_2$ and $\alpha^{+1}(N_2) \subseteq N_1$.

These facts allow us to count the number of neurons in the dataset which could be part of such a two neuron circuit, by counting the number of recorded neurons where another recorded neuron exists, so that one of the facts hold.
Each neuron receives its input either monosynaptically from the inputs or non-monosynaptically via other neurons. These neurons that transmit this input must at least receive the input they are transmitting but with one shorter synaptic linkage. These neurons, which are the minimal requirement for a predecessor neuron, to a neuron N are called the virtual neurons

$$V(N) = \bigcup_{(m,l)\in N} \{(m, l') \mid l' \in \{1, \ldots, l-1\}\} \ .$$

For a neuron N to receive its input completely over a feed forward network in contrast to transmission via network containing loops, for every virtual neuron $N^V \in V(N)$ there must be a matching neuron N' such that the following two conditions hold. The neuron N' receives the input N^V receives, $N^V \subseteq N'$. If N^V transmits its input over n synapses to N then N must contain all inputs that N' receives transmitted over n synapses $\alpha^n(N')$ if the transmitted input at N is excitatory or $\alpha^{-1}(N')$ if the transmitted action at N is inhibitory. This kind of analysis relies on the assumption that only the patterns of convergence that we found exist. It is unlikely that the complete set of connectivity within the spinal cord circuitry was mapped in this study.

Swap Randomization. In order to determine if the associations and graph structures quantified by the measures described in the previous sections are by chance, we compared the measures to datasets generated by swap randomization. The swap randomized datasets are created by virtually swapping inputs between neurons under the following constraints, as previously described(Gionis et al., 2007). Each neuron receives the same number of inputs as in the original dataset. Each input contacts the same number of neurons as in the original dataset. If the measure obtained from the recorded dataset is smaller than the average of the measure on the swap randomized datasets, we call the measure reduced. In the opposite case we call it enhanced. Let M be the value of a measure computed on the recorded dataset. Let a and b be the number of swap randomized datasets where the measure is smaller than M respectively larger than M The significance of the comparison to the swap randomized datasets is computed as the empirical p-value

$$p = \frac{1}{1+n} \min\{a, b+1\} \ ,$$

where $n = 10^7$ is the number of swap randomized datasets.

4. Results

We made 114 intracellular recordings in spinal segments C6-T1 of the decerebrated cat (Figure 1 A). Neurons were recorded at depths between 1.31 mm to 3.92 mm from the dorsal surface of the spinal cord, corresponding to anatomical laminae III-VII (Figure 1 B). Of these spinal interneuron recordings, 68 were in the whole cell mode, the recording quality of which allowed the identification of the amplitude of individual synaptic responses and thus could be included in the synaptic weight analysis. The cells were recorded with mild hyperpolarizing currents of 10 pA to 30 pA to prevent the neurons from spiking, thereby facilitating the analysis of the synaptic responses evoked from the peripheral sensory inputs. The general membrane physiology properties, recorded from a subset of the neurons recorded in the whole cell mode, were previously reported (Spanne et al., 2014).

4.1. Matching the shape of the recorded potentials to synaptic activations

Decerebration allowed the reocrdings to be made *in vivo* without anesthesia, i.e. in a system with spontaneous activity in both the spinal neurons and the sensory afferents, the intracellularly recorded activity was characterized by a high number of spontaneous events (Figure 1 C). These events occasionally summed to sufficient depolarization to trigger discharge of an action potential in the recorded neuron. The spontaneous events were typically found to have a shape that was congruent with other spontaneous

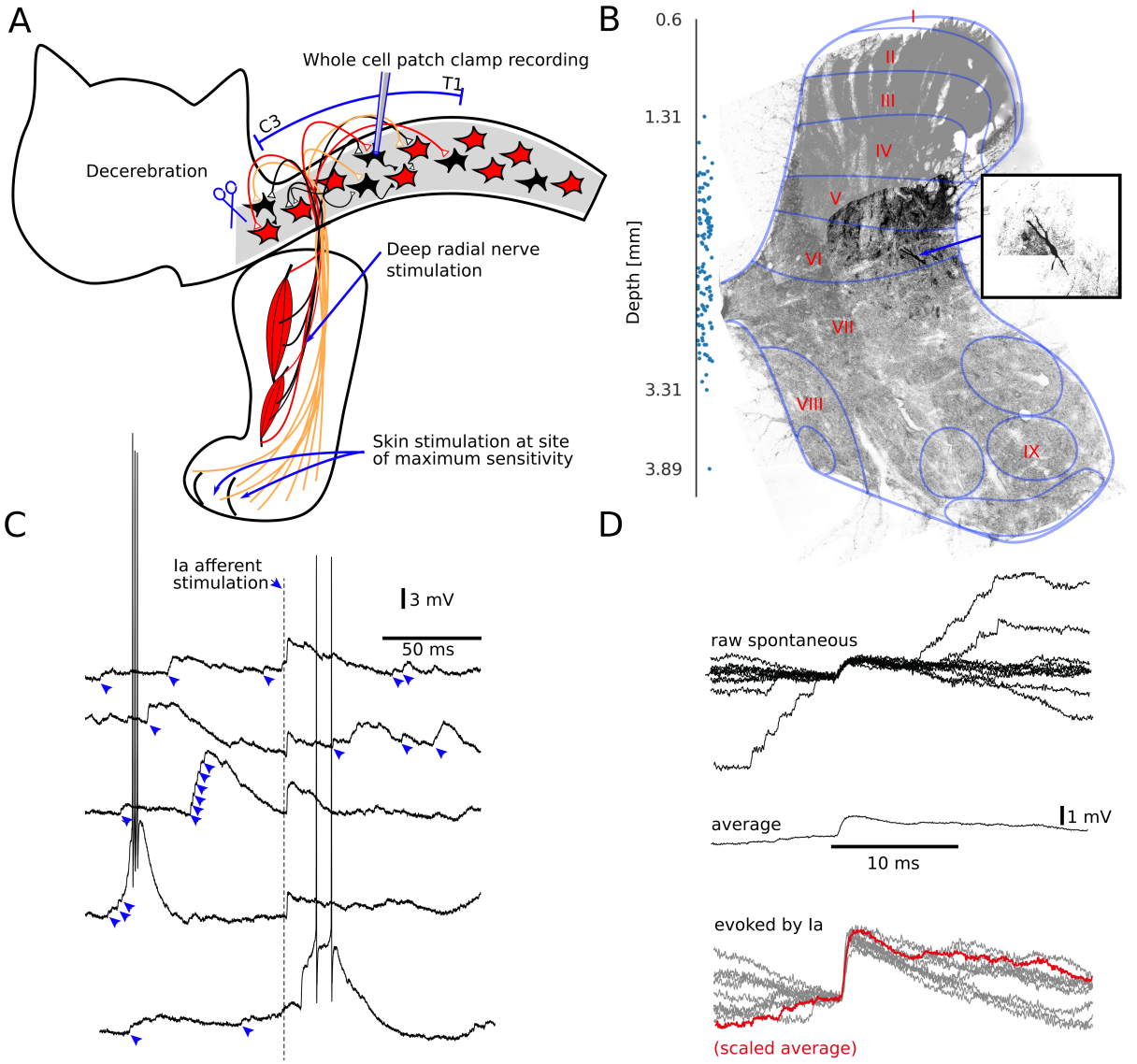

Figure 1: **Experimental setup, location of recorded neurons and unitary EPSPs. A** In vivo preparation, sites of stimulations and recordings. **B** Histological recovery of one recorded neuron with its location in the spinal cord grey matter and a detail image of the recorded neuron with a visible soma and proximal dendrites. The image was acquired by a confocal microscope from a 50 µm thick section from the spinal segment C8. Rexed laminae I-IX are indicated (Rexed, 1952). Additional plot of the depths of each recorded neuron with a random offset in the medial-lateral axis. **C** Five raw traces of recordings from a spinal interneuron (approximate resting $V_m = -60\,\mathrm{mV}$) with near threshold DR stimulation ('Ia afferent stimulation' at dashed vertical line). Blue arrowheads indicate prominent spontaneous EPSP-like responses. The raw traces also illustrate examples of spontaneous spiking, which was reduced by mild hyperpolarizing currents throughout recordings to facilitate the analysis of the evoked synaptic responses. **D** Superimposed spontaneous EPSPs, their average and a comparison between the latter and superimposed EPSP responses evoked by Ia afferent stimulation (DR stimulation at 1.05 times threshold).

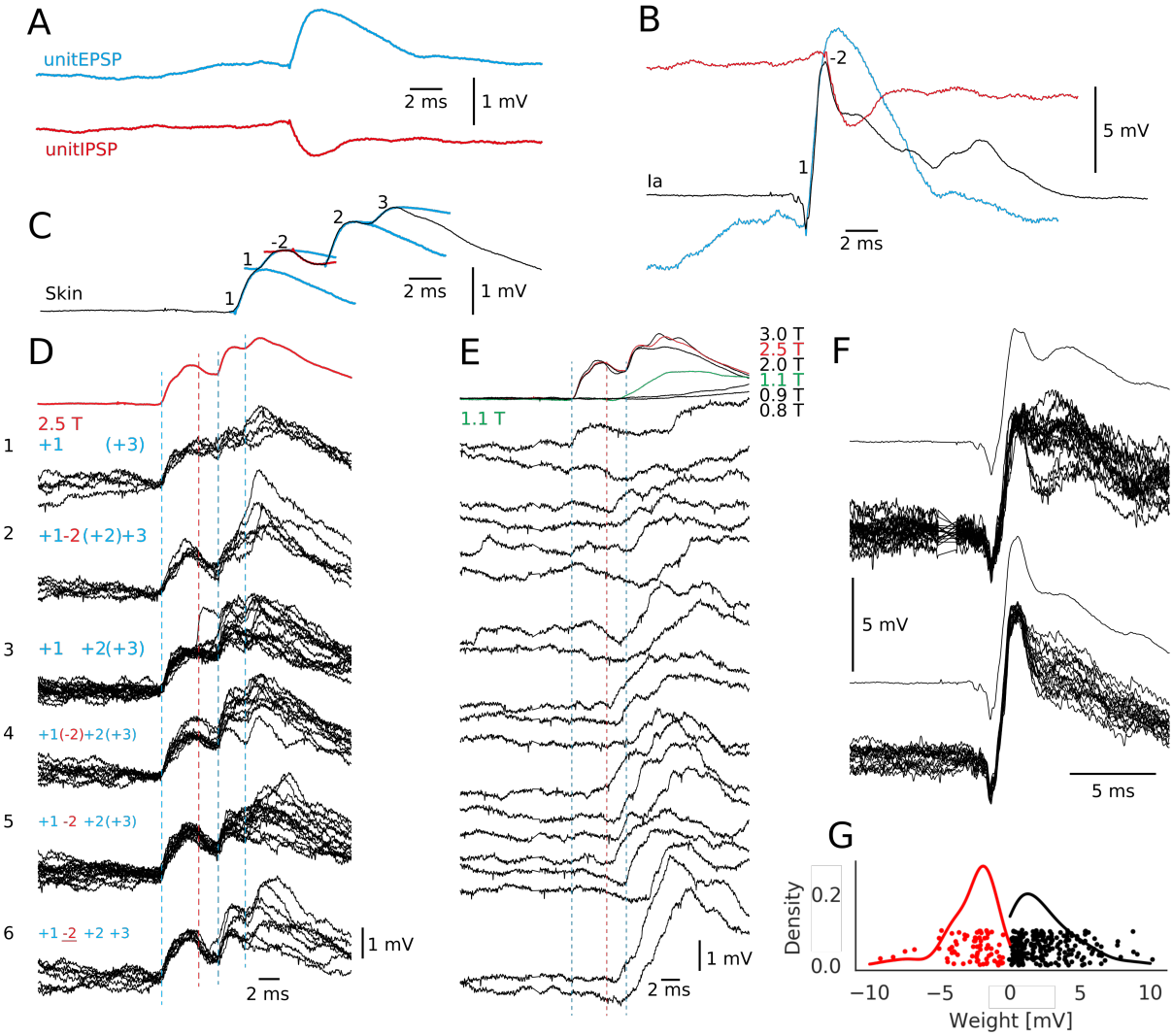

Figure 2:

Figure 2: **Definition of input connectivity based on template reconstruction of sensory-evoked compound synaptic responses** **A** Excitatory PSPs (EPSPs) were averaged to obtain a unit EPSP template. The same was done for inhibitory PSPs (IPSPs). These templates were used to decompose compound evoked synaptic responses. **B** An average PSP response evoked by stimulation of the deep radial nerve (black) that could be decomposed into a (monosynaptic, "1") EPSP and a disyanptic IPSP ("−2") based on amplitude scaling of the PSP templates. **C** Decomposition of an averaged compound synaptic response evoked by skin stimulation. In this sample cell, the response was decomposed into a mono-,di- and trisynaptic EPSP and a disynaptic IPSP. The numbers indicate whether the input was mono-, di-, or trisynaptic, the sign indicates whether it was excitatory or inhibitory **D** Average (red trace) and raw responses evoked by skin stimulation at $2.5T$. Raw traces are grouped by their relative similarity. Brackets around numbers indicate that the specific input was weak, whereas underscored input indicated that the input was strong. **E** Average and raw responses evoked by skin stimulation at $1.1T$. **F** Average and raw responses evoked by DR stimulation. Note that the IPSP partially disappears at the lower DR stimulation intensity. **G** Kernel density estimations of the synaptic weight distributions of excitatory (red) and inhibitory (black) PSPs across all neurons recorded. Additional plot of individual weights with a random offset in the density axis, and a random offset from $\mathcal{U}(-0.5, 0.5)$ in the weight axis.

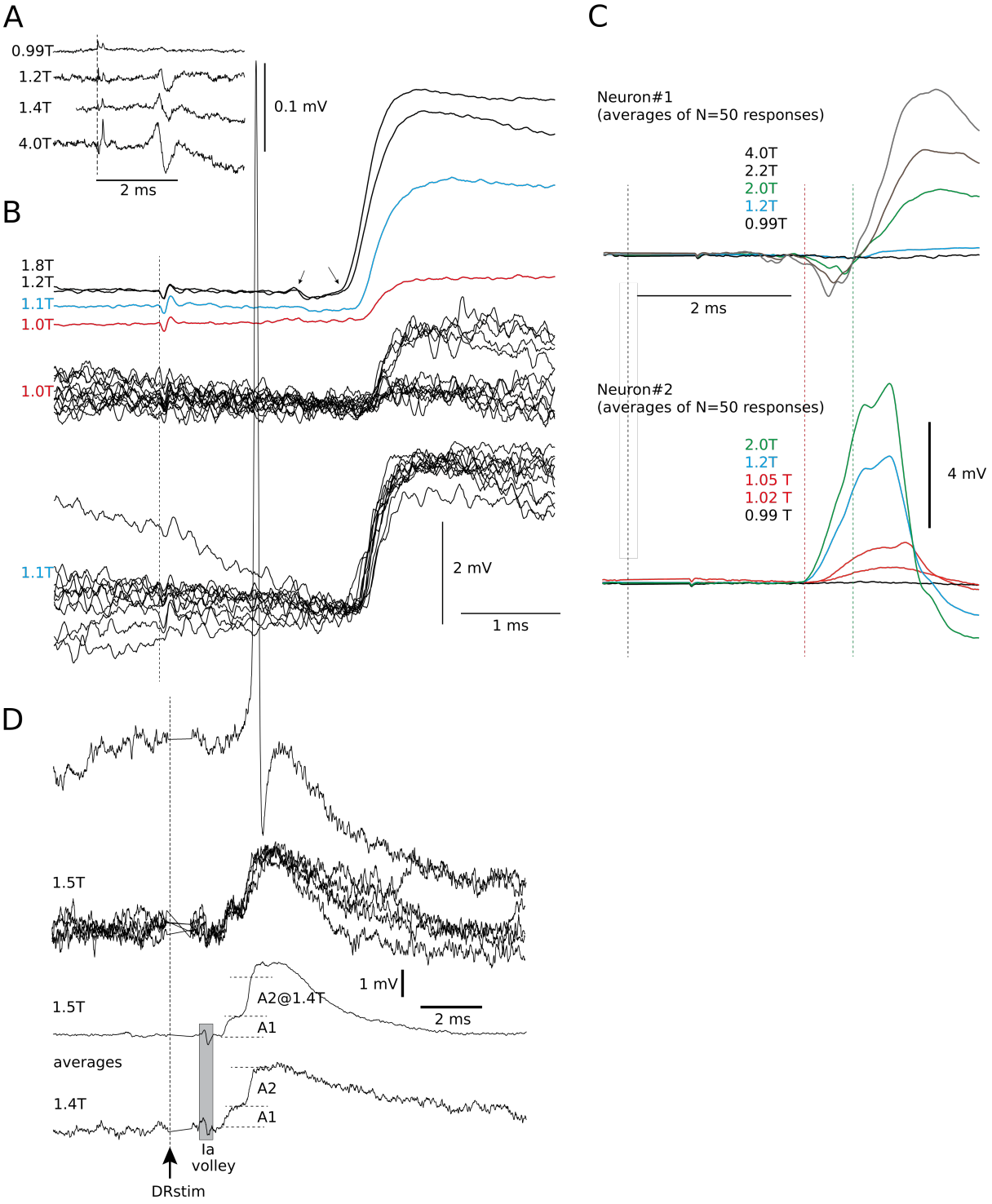
A
0.99T
1.2T
1.4T
4.0T
0.1 mV
2 ms
B
1.8T
1.2T
1.1T
1.0T
1.0T
1.1T
2 mV
1 ms
C
Neuron#1
(averages of N=50 responses)
4.0T
2.2T
2.0T
1.2T
0.99T
2 ms
Neuron#2
(averages of N=50 responses)
2.0T
1.2T
1.05 T
1.02 T
0.99 T
4 mV
D
1.5T
1 mV
2 ms
1.5T
A2@1.4T
A1
averages
A2
1.4T
A1
Ia
volley
DRstim

Figure 3:

Figure 3: **Separation of responses from Ia and Ib afferents activated from the deep radial (DR) nerve.** Black vertical dashed lines indicate the onset of stimulation in all panels of this figure. **A** Definition of threshold intenstity T for activating the Ia afferent nerve volley based on the local field potentials recorded within the spinal grey matter, outside the recorded neurons. Note that the response latency shortens slightly with increased stimulation intensity. **B** From the same experiment after establishing an intracellular recording, EPSPs evoked at and above T. Top, averages of the responses evoked at four different intensities. Arrows indicate the Ia afferent volley and the onset of the EPSP response. Below, superimposed raw responses evoked at $1.0T$ and $1.1T$. **C** From another experiment, average recordings of evoked EPSPs from two different neurons, recorded adjacently in the same electrode track. Neuron#1 responded only at intensities $> 1.2T$, and the EPSPs had a distinctly longer response latency time than the preceding Ia synaptic LFP (starting at the red dashed line). Bottom set of recordings, Neuron#2 responded at all intensities above $0.99T$. Green dashed line indicates response latency time for the evoked EPSP in Neuron#1, red dashed line indicates response latency time for the evoked EPSP in Neuron#2. For Neuron#2, note that the stimulation at higher intensities sometimes evoked a spike, which created the ripple in the later part of those responses. Note that there was no clearly visible Ia volley in these two recordings. **D** Recording from a neuron with monosynaptic input from both Ia and Ib afferents. Top, raw traces evoked at $1.5T$, one of which also contained an evoked spike when the clamping current was released for one of the simulation repetitions. Average of responses at $1.4T$ and $1.5T$ show two summed EPSPs with amplitudes A1 and A2. The amplitude of A1 was the same at $1.4T$ and $1.5T$ but the A2 amplitude was larger at $1.5T$, which alongside the differences in latency times of the two inputs indicate that response A1 was a Ia EPSP and A2 was a Ib EPSP.

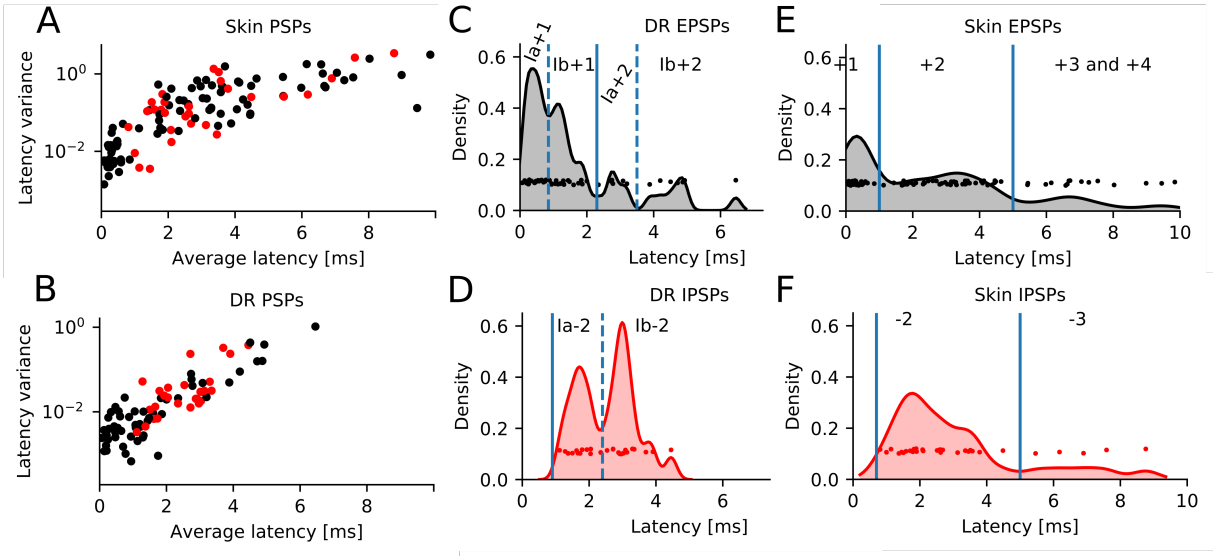

Figure 4: **Definition of input connectivity based on response latency times. A-B** The average response latency time plotted against variance of the response latency time for EPSP (red) and IPSP (black) responses. **C–F** The distribution of the average response latency times of the evoked PSPs for each recorded response component in each neuron (the data points are given a small random offset along the density axis for better visualization of the density). A kernel density estimation of the density of responses at each given response latency time is overlaid on the data points (0.1 ms resolution in **C** and 0.2 ms resolution in **D-F**). Latency times for responses evoked by the DR and the skin stimulation were normalized by subtracting the latency time of the respective LFP. Separation of PSPs evoked by Ia and Ib afferents, respectively, is indicated by dashed blue lines.

events, and they all displayed a voltage-time shape similar to unitary EPSPs recorded in other parts of the central nervous system (Jörntell and Ekerot, 2006; Bengtsson and Jörntell, 2009; Bengtsson et al., 2013). It was more clear when multiple such events were averaged that they had the typical shape of an EPSP (Figure 1 D). Unitary responses evoked using electrical stimulation of peripheral afferents at a sufficiently low intensity (near activation threshold) had the same shape, too. These findings show that the spontaneous events with this shape were EPSPs, which could be triggered by spontaneously active external afferents or other spinal interneurons by electrical activation of peripheral sensory afferents synaptically connected to the recorded neuron.

4.2. Evoked compound PSP responses and mapping of the input connectivity

For each cell recorded we could identify unitary EPSPs and unitary IPSPs (Figure 1D). Averaging multiple such PSPs, detected in the spontaneous activity or evoked by low-intensity afferent stimulation, was used to create template EPSPs and IPSP, respectively (Figure 2A). Using scaling of these template PSPs, we could reconstruct the raw responses evoked by afferent stimulation, where the upscaling of the template PSP would be equivalent to the compound PSP that would result from the simultaneous activation of multiple separate synapses. The scaling of the template PSPs corresponds to the activation of multiple synapses at the same time (Bengtsson et al., 2013). Pure monosynaptic EPSPs were readily identified by their distinct overlap with the template PSP. Template PSPs were constrcutred separately for each neuron recorded. We observed that the time constants of template PSPs could differ somewhat between different neurons, but the differences were not dramatic. Similarly, within each neuron, different spontaneous EPSPs could potentially differ somewhat between different EPSP events, but the template was designed to correspond to the average of these events.

Compound raw responses, resulting from the activation of partly overlapping EPSPs and IPSPs, were analyzed by a template fitting process, i.e. scaling and onset time identification. In Figure 2B and C example results of the fitting process are illustrated for responses evoked by skin input and muscle afferent input, respectively. Since the responses of this neuron to the two inputs were relatively consistent, we could in this illustration apply the template fitting even to the average responses. The analysis was however applied to individual raw traces, using the same principles as illustrated in Figure 2B,C. In Figure 2D-F we show how this method was applied to the single raw traces. In Figure 2D, the exact same stimulus intensity ($2.5T$, average response on top, in red, same as in Figure 2C) evoked six main groups of responses. The earliest part was the monosynaptic response component (+1, first blue dashed vertical line). The monosynaptic response (which actually consisted of two separable components, likely because it contained afferents of two separate mean conduction velocities Bengtsson et al. (2013). The monosynaptic response was essentially invariant across the six groups, i.e. it was evoked at the exact same response latency time with a response amplitude with low variance.

In comparison, di- and trisynaptic responses were more variable with respect to both amplitude and latency (Figure 4 A,B), which is to be expected for non-monosynaptic inputs as the transmission is dependent on the (time-varying) excitability of the intercalated spinal interneurons at the time of sensor activation. Moreover, the intercalated neurons will also lead to the response onset latency times being substantially longer than for the monosynaptic response, as measured from the time of arrival of the afferent input into the spinal cord white matter. This can for example be seen for the disynaptic IPSP (-2, average onset latency time at the red dashed vertical line) which was essentially absent from the responses in groups 1 and 3, and much more prominent in group 6. Later response components (+2 and +3) were also variable in their occurrence, amplitude and response latency times. Figure 2E illustrates the raw responses to a stimulaiton intensity of just above the threshold ($1.1T$). In this case, the monosynaptic EPSP and the disynaptic IPSP essentially did not occur, but the more indirect excitatory synaptic responses remained. In this case, the wildly variable nature of these indirect responses were more clear. Figure 2F illustrates the raw responses evoked from the DR at two different stimulation intensities. At the lower intensity ($1.1T$), the disynaptic IPSP was highly variable, whereas at the higher intensity ($1.2T$), it was more consistently present. In contrast, the monosynaptic EPSP remained constant across both intensities, even though the higher intensity evoked an compound EPSP with a somewhat larger amplitude. For further analysis synaptic weights were measured for each input connection as the average response amplitude. Figure 2 G shows the distribution of these weights across all neurons where the recording quality allowed the amplitude to be measured (236 excitatory and 74 inhibitory inputs in 68 neurons). The weight distribution is skewed which is commonly associated with learnt weights (Barbour et al., 2007).

We used stimulation of the deep radial (DR) nerve, which contains no skin afferents, to stimulate the Ia and the Ib afferents of the supplied muscles, as previously described(Quevedo et al., 2000). Ia and Ib responses could be separated, even though both inputs were activated through the same nerve. The identification of whether a recorded neuron was receiving synaptic inputs from Ia or Ib afferents or both, in some cases, was based on several criteria similar to those previously used in the literature(Bradley and Eccles, 1953; Eccles et al., 1957*a*,*b*; McCrea et al., 1995). Field potential recordings in the extracellular

tissue outside the recorded neuron was used to identify the threshold of the Ia volley, where the Ia volley correspond to the field potential generated by the action potentials of a population of Ia afferents (Figure 3A). Hence, the intensity of the nerve stimulation used could be expressed as multiples of the threshold stimulation T. Monosynaptic inputs could be defined on basis of their very short delay relative to the LFP, corresponding to the activation of the synapses on the spinal neurons, that was initiated about 0.5 ms after the onset of the Ia afferent volley. For the DR stimulation, a neuron activated at $1.0T - 1.1T$ was considered to be activated by Ia afferents (Figure 3B), whereas a neuron that was activated distinctly only above $1.2T$, typically well above this value, was considered to be activated by Ib afferents (Figure 3C). In addition to the threshold criterion, for neurons activated monosynaptically, the responses latency times depended on whether they were activated by Ia or Ib afferents, as defined by the threshold criterion (Figure 3C). These criteria could also be used to identify neurons which had monosynaptic input from both Ia and Ib (Figure 3D).
We also checked whether the repeated activations of afferent input led to changes in the response amplitudes of the evoked PSPs. Over monosynaptic evoked PSPs that appeared at least twenty times at intervals of either 1 s or 334 ms , the average coefficient of variation of the response amplitude was 0.122 ($SD = 0.041$). Also, we could not find any significant evidence of depression or potentiation. A linear fit to the response amplitudes has an average increase of -0.001 mV per stimulation repetition ($SD = 0.01250$).
We next analyzed the response latency times for each identified input, across all neurons. Figure 4A-B show that the responses with longer response latency times also tended to have a higher variance in their response latency times, which is an indication of a response being mediated more indirectly, i.e. over multiple synapses. When analyzing the distribution of the response latency times of the PSPs evoked by the different types of afferents they tended to form clusters. For PSPs that were close to the cluster boundaries, their classifications were additionally confirmed by their stimulation threshold (Figure 3). This formed the basis for determining the input connectivity across all neurons recorded, i.e whether the input connectivity was mono, di or tri-synaptic in addition to whether it was excitatory or inhibitory.

4.3. Clusterability of neurons by input connectivity

We next proceeded by making a systematic analysis of the input connectivity of all recorded neurons. The purpose of the following analysis was to explore if the connectivity across the population formed clusters or classes. First we inspected plots of pairwise weighted input combinations. These input combinations were picked from all recorded inputs that were either monosynaptic excitation or disynaptic inhibition. No classification by input connectivity was immediately obvious in this respect across our set of recorded neurons (Figure 5A), because none of the emerging distributions formed any clusters, but instead rather resembled a continuous single modal distribution. In agreement with a previous report based on more indirect observations (Jankowska and McCrea, 1983) we found neurons with convergent input from Ia and Ib. We also found neurons with convergent inputs from skin and Ia or Ib afferents. Hence, these findings did not indicate any specific rules of input connectivity.
In order to determine in a more standardized fashion if the spinal interneurons could be clustered on basis of their input connectivity, we next utilized the SigClust and GapStatistics tests on the part of the dataset where also the synaptic weights for each input could be defined ($n = 68$ neurons).
The SigClust test (Figure 5 B) can be used to test if a dataset can be split into at least two clusters by comparing the actual data to a number of random samples from a Gaussian distribution fitted to the dataset. If the original dataset has a significantly smaller clustering index (red arrow in Figure 5 than random samples of the Gaussian fit (blue arrows in Figure 5 B), then the SigClust test returns a probability that the dataset is containing clusters. Figure 5 C shows the result of this test on our dataset. The cluster index, which measures how well the dataset can be split into two clusters reported a value of 0.71. The average cluster index of the distribution of random sample datasets was 0.729 with a standard deviation of 0.033. Hence the hypothesis that the dataset was not clusterable could not be rejected ($p = 0.31$).
The GapStatistics test (Figure 5 D) is another method that can be used to test if a dataset can be clustered and in addition it estimates an appropriate number of clusters for the dataset. The appropriate number of clusters is estimated as the point where the gap measure between the dataset and random samples from a fitted uniform distribution is maximized (Figure 5 D). However for our dataset of recorded neurons the gap continued to increase with increasing number of clusters (Figure 5 E). When the gap just continues to grow with the number of datapoints added, as in this case, it indicates that the data does not contain any clusters. Hence, all of these three analyses indicated indicated that the input connectivity of the spinal interneurons did not contain any clusters, i.e. our population of neurons did not contain any specific input connectivity classes.

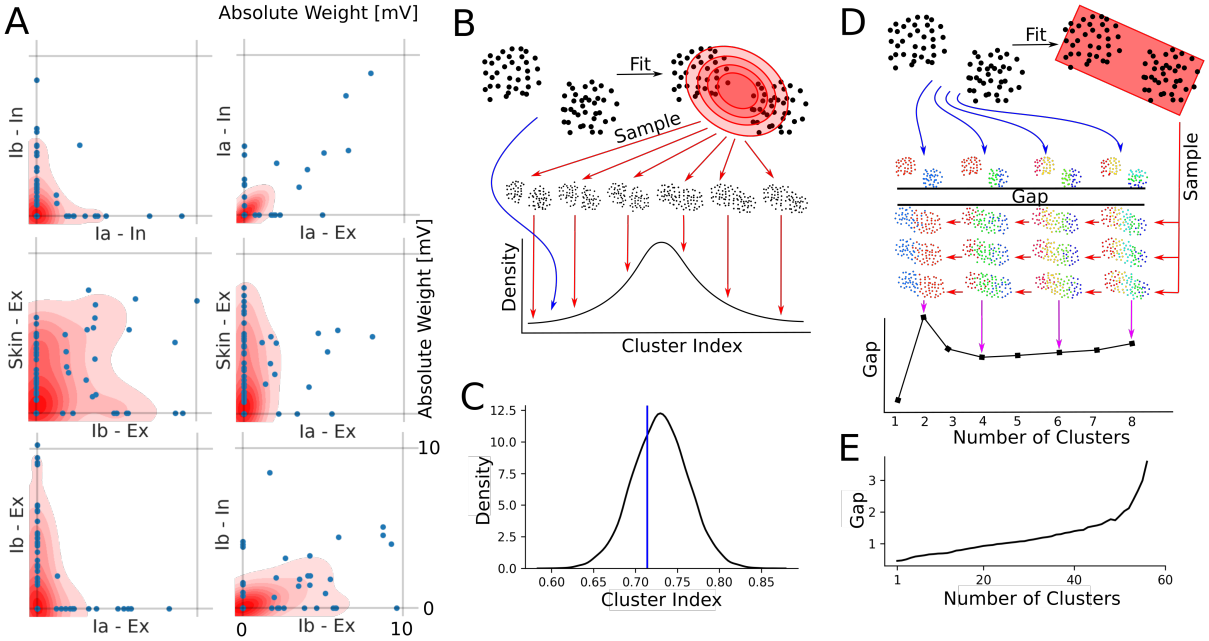

Figure 5: **Absence of correlation patterns and clusterability of neurons by input combinations.** **A** Kernel density estimations of absolute synaptic weights from distinct combinations of monosynaptic excitatory and disynaptic inhibitory inputs. (In: Inhibitory, Ex: Excitatory) No subdivision between the neurons is visible, though for some combinations (Ia-In, Ia-Ex) there appears to be some correlation. Additional plot of nonzero input weights at a random offset from $\mathcal{U}(-0.5, 0.5)$. **B** Illustration of analysis method and the output of the SigClust test expected for a hypothetical dataset with clusters. The clustering index of the original dataset (red arrow) is compared to that of random samples from a Gaussian distribution (blue arrows) fitted to the dataset (black arrow). **C** The SigClust results for our set of recorded neurons. The clustering index for the dataset of recorded neurons (blue line) compared to the fitted Gaussian distribution (black). **D** Illustration of the GapStat analysis method and expected output for a hypothetical dataset with two clusters. GapStat method for a hypothetical case of a dataset with two clusters. The GapStat method first fits a uniform distribution to the data. The samples are drawn from that distribution (blue arrows) and for each possible number of clusters the gap to the actual dataset (red arrows) is computed. The number of clusters at which the gap to the actual dataset is maximized is the estimated number of clusters for the dataset. **E** The GapStat results for our set of recorded neurons. The plot illustrates that the gap just continues to grow with the number of tested clusters. Hence this method does not find our data clusterable.

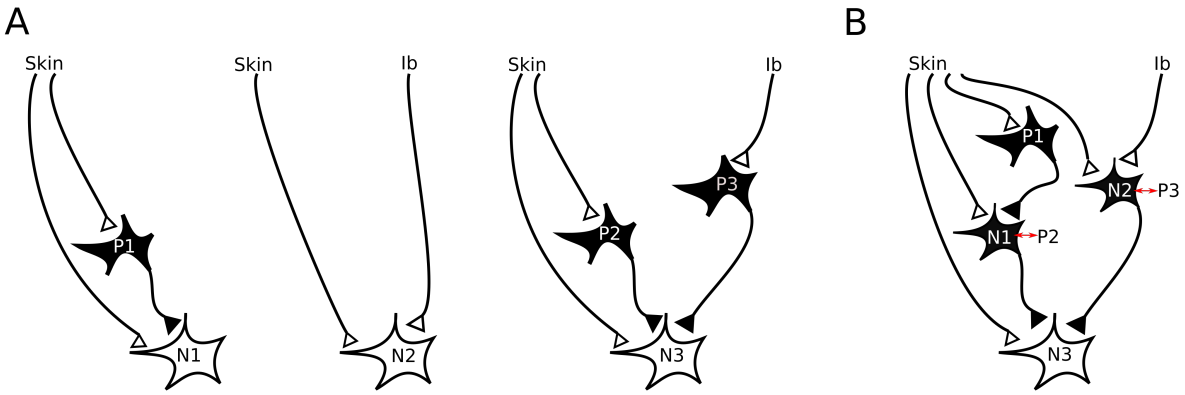

Figure 6: **Matches between the input connectivity of individual target neurons and predecessor neurons explain all inputs observed. (A)** Input connectivity of three recorded neurons $N1$,$N2$ and $N3$. **(B)** The input connectivity of neuron $N3$ can be explained by the input connectivity of neurons $N1$ and $N2$.

4.4. Spinal network structure

Given that our data provided input connectivity data also for indirect, non-monosynaptic inputs, it implied that some of the neurons recorded from could be responsible for mediating the indirect input to other neurons recorded from. Hence, we also tested if the input connectivity observed across the full population of neurons ($n = 114$) could be explained by the pool of recorded input connectivity data. We first tested if the recorded input connectivity could be explained by a pure feed-forward network.

We did this by reconstructing a hypothetical feed forward network, for all recorded input combinations observed up to four sequential synapses away from the monosynaptic sensory input source. This analaysis built on the principle shown in Figure 6 for three exemplary neurons, i.e. for any neuron receiving non-monosynaptic input, there must be predecessor neuron(s), which mediate(s) that input.

Figure 6A shows the input connectivity for three of our recorded neurons $N1$,$N2$ and $N3$. Neuron $N1$ received excitatory monosynaptic input from Skin and disynaptic inhibitory input from Skin. For the inhibitory input an inhibitory interneuron (Neuron $P1$) is necessary. Neuron $N2$ received monosynaptic excitatory input from Skin and Ib. Neuron $N3$ received the same input as $N1$ plus disynaptic inhibition from Ib. The inhibitory input to $N3$ could then have been provided by the two inhibitory interneurons $P2$ and $P3$. The input connectivity of Neuron $N3$ can be explained by the input connectivity of neurons $N1$ and $N2$. If the neuron $N1$ would be assumed to be an inhibitory interneuron, then it could correspond to neuron $P2$. If the neuron $N2$ would be assumed to be an inhibitory interneuron, then it could correspond to neuron $P3$. (Figure 6B).

Hence, the network connectivity pattern observed in these three recorded interneurons could be readily explained by our recording data. Note that the presence of $P1$ would not be possible to detect through the $N3$ recording, as disinhibitory effects were not detectable, but its presence could be detected by the $N1$ recording. For all but one of our recorded neurons, the input connectivity to each neuron could in each case be explained by a recorded predessor neuron, where a valid predecessor contained the necessary input and in addition did not mediate input that was not observed in the recorded neuron. Therefore, all recorded patterns of input connectivity could be explained by monosynaptic inputs plus the inputs observed in other neurons in our data. Most of these connections were likely to be of a feed-forward type, athough, due to the lack of input classes, there were no indications of any specific layers within the spinal cord circuitry.

Using a similar approach, we found that the number of potential disynaptic excitatory loop connections in our recorded connectivity data was significantly reduced ($p < 0.05$) compared to chance (Figure 7).

4.5. Associations between neuronal inputs

Since correlations and anticorrelations in the input connectivity were visible in the analysis above (for instance a possible linear relation between Ia-Ex and Ia-In in Figure 5A), we searched for any possible correlation or anticorrelation in the inputs systematically, using an association rule analysis.

In our data, a spinal interneuron could receive input from the Ia, the Ib and the skin afferents as IPSPs and/or as EPSPs. Note that this part of the analysis ignored whether the input was mono-, di-, tri- or quadsynaptic. Since only the binary absence or presence of input was considered, and not the weights of the inputs, the full dataset of 114 neurons was used.

We tested if any of the resulting thirty possible input combinations (associations) were significantly enhanced or reduced compared to a random distribution (Figure 8), where the random distribution was generated by swap randomizing the input combinations of our dataset (Figure 8A). The position of the

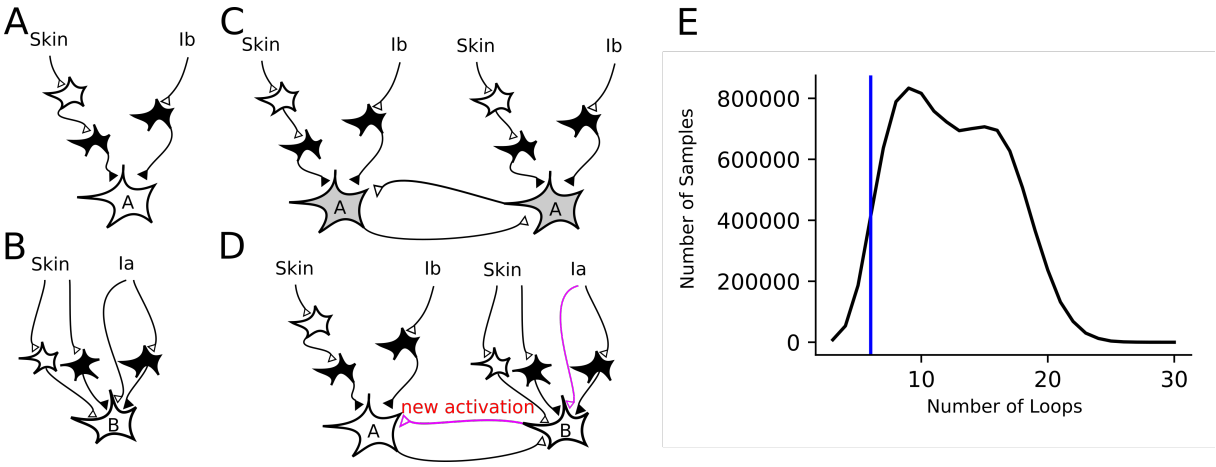

Figure 7: **Disynaptic excitatory loops were suppressed compared to chance. A,B** Two example input combinations. **C** Two neurons with input combination A could potentially be connected to each other as our recording data could not detect inhibited synaptic excitation. **D** Neurons with input combinations A and B could not be connected to each other as the added disynaptic Ia excitation (as well as added trisynaptic skin excitation) would have been detected in our recording data. Hence, we can use our recording data to estimate the number of potential reciprocal excitatory loops. **E** Comparison of the observed number of potential excitatory loops in the recorded data (blue line) compared to the swap randomized datasets. Reciprocal excitation was significantly reduced ($p < 0.05$) compared to chance, i.e. the swap randomized dataset of connectivity.

recorded data in relation to the distribution of this randomized data was used to indicate if the presence of each specific connectivity pattern was enhanced or reduced compared to chance connectivity.
The threshold of significance for each test was adjusted so that the total significance of all tests was $p = 0.05$. For both the Ia afferents, the Ib afferents and the skin input, the associations between inhibition and excitation were significantly enhanced (Figure 8B, green panels). The association between inhibitory input from the skin and Ia afferents were significantly enhanced (green panel). None of the other input combinations were found to be reduced or enhanced at a significant level (grey panels). Hence, the assocation rule analysis suggested that overall there were limited constraints on the input combinations observed in our set of recorded spinal interneurons.

5. Discussion

We made intracellular recordings from a variety of spinal interneurons in the lower cervical segments *in vivo* and recorded their synaptic input connectivity from a variety of input sources and defined the synaptic linkages by which the inputs were provided. We found that although the inputs to the individual spinal interneuron were well organized, with large to very large compound synaptic responses for the input that was present but absent or very weak input for all other synaptic input connectivities, across the population of spinal interneurons the synaptic input patterns formed a great diversity. This diversity of input connectivities provided no support for specific sets of spinal interneuron classes with respect to their inputs. Instead, the patterns of input connectivity to the spinal interneurons was better described as a continuum. The only exceptions were a reduced association between Ia and Ib excitation and an enhanced association between excitation and inhibition for inputs from the same source (Ia, Ib and skin). As discussed below, a spinal cord with a continuum of input combinations, rather than a limited set of fixed entities, indicate that much of the connectivity is most likely shaped through learning, which carries the advantage of making the spinal cord circuitry better geared to cope with complex motor tasks and flexibility in motor control.

5.1. Methodological considerations

Since we kept the skin almost entirely intact (except for small incision around the DR nerve), we could manually identify the skin area of maximum sensitivity for each recorded interneuron and place stimulation electrodes into that part of the skin to detect its synaptic input to the recorded spinal interneuron. It is known that each spinal interneuron can receive different types of synaptic inputs from different skin areas (Weng and Schouenborg, 1996), so in this respect we have underestimated the complexity of the skin input connectivity to these neurons. Moreover, because of our requirement to keep the skin as intact as possible, an experimental short-coming was that we could only use the DR nerve for stimulation of muscle afferents. The DR nerve supplies a high number of muscles in the forearm and paw, but not all. Hence, there were several muscles for which we could not test the presence of muscle afferent input. Also, we could not be certain that the inputs provided from Ia and Ib afferents, and excitatory versus

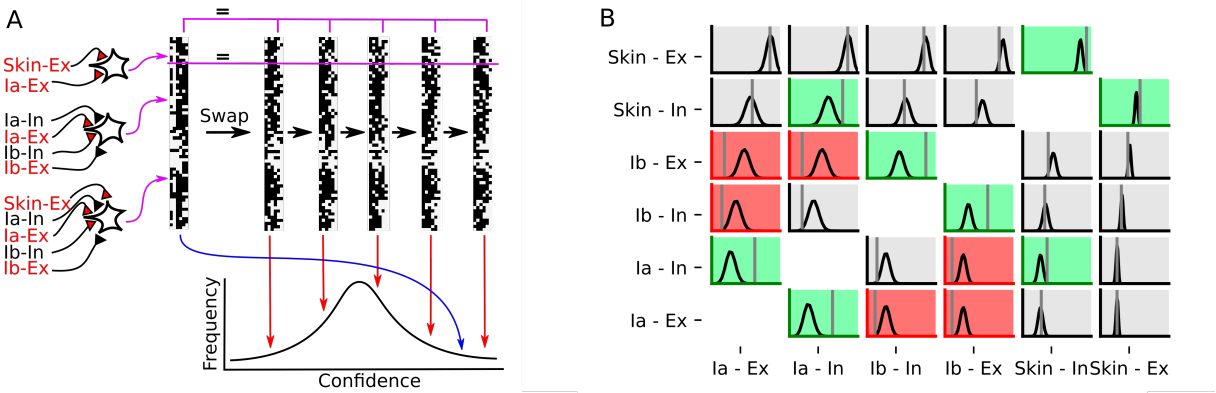

Figure 8: **Estimation of the observed input combinations compared to chance. A** The input connectivity of the recorded neurons is represented as a matrix of binary elements (left column) where each line represents the input to one recorded neuron. In this analysis, we only considered input from the three main sensory sources and whether the input was excitatory or inhibitory. Swap randomization was used to construct random matrices with equal number of connections as in the observed data for each respective neuron. The scrambled data is used to build a distribution of random connectivities (red arrows) against which the confidence of the recorded connectivity patterns can be compared (blue arrow). **B** For each possible combination of inputs, the confidence of the specific input combination of the data versus the distribution of confidence of the swap randomized data is shown. Associations that are significantly enhanced are marked green, significantly reduced associations are marked red. Input combinations that were not significantly enhanced or reduced are shown in grey. The individual significance tests are corrected for multiple comparisons such that the total significance level is at 0.05.

inhibitory synaptic inputs, were from the same muscle or not, and interactions between antagonists and agonists could also not be studied. Therefore, even though our data show a highly complex connectivity, it is clear that our data represents an underestimate of that complexity.

Our *in vivo* intracellular recordings provided many advantages for the study of the physiological connectivity (i.e. anatomical connectivity combined with the weights of the synaptic inputs) of the fully developed mammalian spinal cord. First, whereas an acute in vivo preparation was necessary to obtain long-term intracellular recordings in such a difficult area as the spinal cord, decerebration rather than anesthesia provided the advantage that anesthesia-induced suppression of neural and synaptic activity was omitted and hence also low strength synaptic responses with multiple synaptic relays could be more reliably recorded. The low recording noise of the whole cell patch clamp technique also provided substantial advantages regarding the resolution of the recordings, where for example even unitary synaptic potentials can be recorded, compared to the classical neurophysiological recordings where such weaker inputs would have been at substantially higher risk of being missed. The combination of these two methodological advantages could be a main explanation for why we could see a continuum in the synaptic input connectivity rather than distinct classes of interneurons in terms of their inputs.

5.2. Relation to the classical neurophysiological literature

In our data one could see traces hinting at a classification scheme, based on input connectivity. For instance, the concept of separated Ia interneurons and Ib interneurons could have arisen as a consequence of the fact that we found convergent connections of Ia and Ib afferents to be reduced compared to chance (Figure 8). Although indirect observations of convergence between Ia and Ib afferents in spinal interneurons have been reported previously (Jankowska and McCrea, 1983). In our data, these interneurons no longer formed distinct classes but instead formed a continuum (Figure 5). An explanation that comes in addition to the methodological issues described above could be that we did not actively look for specific neuron types, and that we therefore did not find them. Moreover, we found extensive convergence between cutaneous and proprioceptive afferents, where the organization of cutaneous afferent inputs is considered to be a major remaining gap in the understanding of spinal motor systems (Loeb and Tsianos, 2015). While it has been noted that spinal interneurons can receive cutaneous inputs in addition to proprioceptive inputs, the cutaneous inputs have typically been grouped under the flexor reflex afferent (FRA) concept (Jankowska, 1992; McCrea, 1992). Hence, their contribution to the spinal cord connectivity has not been explored in great detail except for the topographical organization of cutaneous afferent inputs to the spinal cord (Levinsson et al., 2002) and the input-output relationship between skin input and controlled movement (Petersson et al., 2003).

5.3. Relation to classification schemes proposed based on gene expression patterns

More recently, a classification scheme for spinal interneurons has been proposed based on their gene expression associated with the initiation of spinal interneuron differentiation in embryonic development

(Alstermark and Isa, 2012; Zampieri et al., 2014; Azim et al., 2014; Gabitto et al., 2016). These genetic classes have been associated with function and involvement in specific tasks. Additionally, matches between the classical neurophysiological input classification scheme with the genetic classification scheme have been suggested to exist (Brownstone and Bui, 2010; Bikoff, 2019). However, what would seem a significant caveat to the notion of a genetically predefined wiring of the spinal interneuron circuitry is that the equivalent of the spinal cord developed 420 million years ago, when the phylogenetic line leading to mammalians diverged from the elasmobranchs (Grillner, 2018; Jung et al., 2018). It was noted that "the skate spinal cord has the same interneuronal building blocks available to form the locomotor network as seen in mammals" (Grillner, 2018), which encompasses animals of a great variety of non-overlapping movement patterns. Furthermore, the spinal cord circuitry is able to adapt to such dramatic biomechanical changes as a reconfiguration of the arrangement of muscles (Loeb, 1999). Such observations indicate that if there is a genetic pre-configuration of the spinal cord circuitry, it must be possible to overwrite even during the adult life span. Further evidence is that the distribution of afferent fibers is correlated with the usage of muscles (Fritz et al., 1989). Moreover, even developmental afferent wiring in the dorsal horn is activity dependent (Granmo et al., 2008), which indicates that even early structuring of the spinal cord circuitry is to a large extent influenced by learning and activity.

5.4. Implications for the functional interpretation of the spinal cord circuitry

Our findings suggest that the connectivity of the spinal interneuron circuitry can to a large extent be explained as a consequence of learning, because each interneuron received strong responses for some input sources and some synaptic linkages of those inputs, whereas other inputs, present in other interneurons, were absent. Because of the diversity of input patterns observed across the population of interneurons, these findings suggest learnt rather than innate patterns of connectivity, though a combination of the two can of course not be ruled out by the present set of experiments.

An important consequence of learning is that the circuitry becomes more adaptable to the biomechanical properties of the body. A previous spinal cord model was constructed using the limited number of spinal neuron classes defined in the literature. Already this type of spinal cord system provides the possibility to generate a great diversity of temporally coherent movements using simple descending control (Raphael et al., 2010). To rebuild such a model without neuron classes and instead with a focus on a diversity of input connections would be expected to perform at least as good in this respect, because all neurons that would be representative for a class would still be present in addition to a wide diversity of other input connectivities. Such diversity of connectivities could enrich the repertoire of possible muscle activation patterns and could help resolve long standing controversies around synergy control (Tresch and Jarc, 2009). Whereas the dominant solutions in the spinal cord circuitry to descending motor commands would equal our most commonly observed movement patterns or synergies (Santello et al., 2013) a great variety of spinal interneurons would help preventing the system from getting stuck in only those movement patterns and provide the motor control systems of the CNS with a major potential flexibility to generate movements that are still coherent and organized.

6. Acknowledgments

This research received funding from the German Aerospace Center under the research and development contracts D / 572 / 67 24 68 70, D / 572 / 67 27 00 80, the European Union's Horizon 2020 Framework Programme for Research and Innovation under the Specific Grant Agreements No. 720270 (Human Brain Project SGA1), 785907 (Human Brain Project SGA2), 945539 (Human Brain Project SGA3), the Hand Embodied (THE) (an Integrated Project funded by the EU under FP7, project no. 248587) and the Swedish Research Council.

7. Author Contribution

Conceptualization, H.J., F.B., A.A.S.; Methodology, H.J., F.B., A.A.S., M.K., P.S.; Software – Network Structure, M.K.; Software – Association Rules, M.K.; Formal Analysis, H.J., M.K., P.S.; Investigation, H.J., F.B.; Writing – Original Draft, H.J., M.K.; Writing – Review & Editing, H.J., M.K., P.S., A.A.S.; Supervision, H.J., A.A.S.; Funding Acquisition, A.A.S., F.R., H.J., A.K.;

8. Declaration of Interests

The authors declare no competing interests.

Agrawal, R., Imieliński, T. and Swami, A. (1993), Mining association rules between sets of items in large databases, *in* 'Proceedings of the 1993 ACM SIGMOD international conference on Management of data', pp. 207–216.

Alstermark, B. and Isa, T. (2012), 'Circuits for skilled reaching and grasping', *Annual review of neuroscience* **35**, 559–578.

Azim, E., Jiang, J., Alstermark, B. and Jessell, T. M. (2014), 'Skilled reaching relies on a v2a propriospinal internal copy circuit', *Nature* **508**(7496), 357.

Barbour, B., Brunel, N., Hakim, V. and Nadal, J.-P. (2007), 'What can we learn from synaptic weight distributions?', *TRENDS in Neurosciences* **30**(12), 622–629.

Bengtsson, F., Brasselet, R., Johansson, R. S., Arleo, A. and Jörntell, H. (2013), 'Integration of sensory quanta in cuneate nucleus neurons in vivo', *PloS one* **8**(2), e56630.

Bengtsson, F. and Jörntell, H. (2009), 'Sensory transmission in cerebellar granule cells relies on similarly coded mossy fiber inputs', *Proceedings of the National Academy of Sciences* **106**(7), 2389–2394.

Bikoff, J. B. (2019), 'Interneuron diversity and function in the spinal motor system', *Current Opinion in Physiology* **8**, 36–43.

Bradley, K. and Eccles, J. C. (1953), 'Analysis of the fast afferent impulses from thigh muscles', *The Journal of physiology* **122**(3), 462–473.

Brownstone, R. M. and Bui, T. V. (2010), 'Spinal interneurons providing input to the final common path during locomotion', *Progress in brain research* **187**, 81–95.

Bui, T. V., Akay, T., Loubani, O., Hnasko, T. S., Jessell, T. M. and Brownstone, R. M. (2013), 'Circuits for grasping: spinal di3 interneurons mediate cutaneous control of motor behavior', *Neuron* **78**(1), 191–204.

Burstein, M. D., Tsimelzon, A., Poage, G. M., Covington, K. R., Contreras, A., Fuqua, S. A., Savage, M. I., Osborne, C. K., Hilsenbeck, S. G., Chang, J. C. et al. (2015), 'Comprehensive genomic analysis identifies novel subtypes and targets of triple-negative breast cancer', *Clinical Cancer Research* **21**(7), 1688–1698.

Chen, A. I., de Nooij, J. C. and Jessell, T. M. (2006), 'Graded activity of transcription factor runx3 specifies the laminar termination pattern of sensory axons in the developing spinal cord', *Neuron* **49**(3), 395 – 408.

Chiaravalloti, N. D., Weber, E., Wylie, G., Dyson-Hudson, T. and Wecht, J. M. (2020), 'Patterns of cognitive deficits in persons with spinal cord injury as compared with both age-matched and older individuals without spinal cord injury', *The journal of spinal cord medicine* **43**(1), 88–97.

Crone, S. A., Quinlan, K. A., Zagoraiou, L., Droho, S., Restrepo, C. E., Lundfald, L., Endo, T., Setlak, J., Jessell, T. M., Kiehn, O. et al. (2008), 'Genetic ablation of v2a ipsilateral interneurons disrupts left-right locomotor coordination in mammalian spinal cord', *Neuron* **60**(1), 70–83.

Diamond, A. (2000), 'Close interrelation of motor development and cognitive development and of the cerebellum and prefrontal cortex', *Child Development* **71**(1), 44–56.

Eccles, J. C., Eccles, R. M. and Lundberg, A. (1957*a*), 'Synaptic actions on motoneurones caused by impulses in golgi tendon organ afferents', *The Journal of Physiology* **138**(2), 227–252.

Eccles, J. C., Eccles, R. M. and Lundberg, A. (1957*b*), 'Synaptic actions on motoneurones in relation to the two components of the group i muscle afferent volley', *The Journal of physiology* **136**(3), 527–546.

Eccles, J. C., Fatt, P. and Koketsu, K. (1954), 'Cholinergic and inhibitory synapses in a pathway from motor-axon collaterals to motoneurones', *The Journal of physiology* **126**(3), 524–562.

Fritz, N., Illert, M., de la Motte, S., Reeh, P. and Saggau, P. (1989), 'Pattern of monosynaptic ia connections in the cat forelimb.', *The Journal of physiology* **419**(1), 321–351.

Gabitto, M. I., Pakman, A., Bikoff, J. B., Abbott, L., Jessell, T. M. and Paninski, L. (2016), 'Bayesian sparse regression analysis documents the diversity of spinal inhibitory interneurons', *Cell* **165**(1), 220–233.

Gionis, A., Mannila, H., Mielikäinen, T. and Tsaparas, P. (2007), 'Assessing data mining results via swap randomization', *ACM Trans. Knowl. Discov. Data* **1**(3).

Goulding, M. (2009), 'Circuits controlling vertebrate locomotion: moving in a new direction', *Nature Reviews Neuroscience* **10**(7), 507.

Granmo, M., Petersson, P. and Schouenborg, J. (2008), 'Action-based body maps in the spinal cord emerge from a transitory floating organization', *Journal of Neuroscience* **28**(21), 5494–5503.

Grillner, S. (2018), 'Evolution: vertebrate limb control over 420 million years', *Current Biology* **28**(4), R162–R164.

Grün, D., Lyubimova, A., Kester, L., Wiebrands, K., Basak, O., Sasaki, N., Clevers, H. and van Oudenaarden, A. (2015), 'Single-cell messenger rna sequencing reveals rare intestinal cell types', *Nature* **525**(7568), 251.

Hultborn, H. (2001), 'State-dependent modulation of sensory feedback', *The Journal of physiology* **533**(1), 5–13.

Hultborn, H., Jankowska, E. and Lindström, S. (1971), 'Recurrent inhibition of interneurones monosynaptically activated from group ia afferents', *The Journal of Physiology* **215**(3), 613–636.

Jankowska, E. (1992), 'Interneuronal relay in spinal pathways from proprioceptors', *Progress in neurobiology* **38**(4), 335–378.

Jankowska, E. and Edgley, S. A. (2010), 'Functional subdivision of feline spinal interneurons in reflex pathways from group ib and ii muscle afferents; an update', *European Journal of Neuroscience* **32**(6), 881–893.

Jankowska, E. and McCrea, D. (1983), 'Shared reflex pathways from ib tendon organ afferents and ia muscle spindle afferents in the cat.', *The Journal of Physiology* **338**(1), 99–111.

Jessell, T. M. (2000), 'Neuronal specification in the spinal cord: inductive signals and transcriptional codes', *Nature Reviews Genetics* **1**(1), 20.

Jörntell, H. and Ekerot, C.-F. (2002), 'Reciprocal bidirectional plasticity of parallel fiber receptive fields in cerebellar purkinje cells and their afferent interneurons', *Neuron* **34**(5), 797–806.

Jörntell, H. and Ekerot, C.-F. (2006), 'Properties of somatosensory synaptic integration in cerebellar granule cells in vivo', *Journal of Neuroscience* **26**(45), 11786–11797.

Jung, H., Baek, M., D'Elia, K. P., Boisvert, C., Currie, P. D., Tay, B.-H., Venkatesh, B., Brown, S. M., Heguy, A., Schoppik, D. et al. (2018), 'The ancient origins of neural substrates for land walking', *Cell* **172**(4), 667–682.

Levinsson, A., Holmberg, H., Broman, J., Zhang, M. and Schouenborg, J. (2002), 'Spinal sensorimotor transformation: relation between cutaneous somatotopy and a reflex network', *Journal of Neuroscience* **22**(18), 8170–8182.

Liu, Y., Hayes, D. N., Nobel, A. and Marron, J. S. (2008), 'Statistical significance of clustering for high-dimension, low-sample size data', *Journal of the American Statistical Association* **103**(483), 1281–1293.

Loeb, G. E. (1999), 'Asymmetry of hindlimb muscle activity and cutaneous reflexes after tendon transfers in kittens', *Journal of Neurophysiology* **82**(6), 3392–3405. PMID: 10601470.

Loeb, G. E. and Tsianos, G. A. (2015), 'Major remaining gaps in models of sensorimotor systems', *Frontiers in Computational Neuroscience* **9**, 70.

Maechler, M., Rousseeuw, P., Struyf, A., Hubert, M. and Hornik, K. (2019), *cluster: Cluster Analysis Basics and Extensions*. R package version 2.1.0 — For new features, see the 'Changelog' file (in the package source).

McCrea, D. (1992), 'Can sense be made of spinal interneuron circuits?', *Behavioral and Brain Sciences* **15**, 633–633.

McCrea, D., Shefchyk, S., Stephens, M. and Pearson, K. (1995), 'Disynaptic group i excitation of synergist ankle extensor motoneurones during fictive locomotion in the cat.', *The Journal of Physiology* **487**(2), 527–539.

Niedermayer, E. and Lopes Da Silva, F. (1993), *Electroencephalography: Basic Principles, Clinical Applications, and Related Fields.*, Baltimore, MD: Williams and Wilkins.

Pecho-Vrieseling, E., Sigrist, M., Yoshida, Y., Jessell, T. M. and Arber, S. (2009), 'Specificity of sensory–motor connections encoded by sema3e–plxnd1 recognition', *Nature* **459**(7248), 842.

Petersson, P., Waldenström, A., Fåhraeus, C. and Schouenborg, J. (2003), 'Spontaneous muscle twitches during sleep guide spinal self-organization', *Nature* **424**(6944), 72.

Prat, A., Parker, J. S., Karginova, O., Fan, C., Livasy, C., Herschkowitz, J. I., He, X. and Perou, C. M. (2010), 'Phenotypic and molecular characterization of the claudin-low intrinsic subtype of breast cancer', *Breast cancer research* **12**(5), R68.

Quevedo, J., Fedirchuk, B., Gosgnach, S. and McCrea, D. (2000), 'Group i disynaptic excitation of cat hindlimb flexor and bifunctional motoneurones during fictive locomotion', *The Journal of physiology* **525**(2), 549–564.

Raphael, G., Tsianos, G. A. and Loeb, G. E. (2010), 'Spinal-like regulator facilitates control of a two-degree-of-freedom wrist', *Journal of Neuroscience* **30**(28), 9431–9444.

Rexed, B. (1952), 'The cytoarchitectonic organization of the spinal cord in the cat', *Journal of Comparative Neurology* **96**(3), 415–495.

Rongala, U. B., Spanne, A., Mazzoni, A., Bengtsson, F., Oddo, C. M. and Jörntell, H. (2018), 'Intracellular dynamics in cuneate nucleus neurons support self-stabilizing learning of generalizable tactile representations', *Frontiers in cellular neuroscience* **12**.

Santello, M., Baud-Bovy, G. and Jörntell, H. (2013), 'Neural bases of hand synergies', *Frontiers in computational neuroscience* **7**, 23.

Spanne, A., Geborek, P., Bengtsson, F. and Jörntell, H. (2014), 'Spike generation estimated from stationary spike trains in a variety of neurons in vivo', *Frontiers in Cellular Neuroscience* **8**.

Tibshirani, R., Walther, G. and Hastie, T. (2001), 'Estimating the number of clusters in a data set via the gap statistic', *Journal of the Royal Statistical Society: Series B (Statistical Methodology)* **63**(2), 411–423.

Tothill, R. W., Tinker, A. V., George, J., Brown, R., Fox, S. B., Lade, S., Johnson, D. S., Trivett, M. K., Etemadmoghadam, D., Locandro, B. et al. (2008), 'Novel molecular subtypes of serous and endometrioid ovarian cancer linked to clinical outcome', *Clinical cancer research* **14**(16), 5198–5208.

Tresch, M. C. and Jarc, A. (2009), 'The case for and against muscle synergies', *Current opinion in neurobiology* **19**(6), 601–607.

Verhaak, R. G., Hoadley, K. A., Purdom, E., Wang, V., Qi, Y., Wilkerson, M. D., Miller, C. R., Ding, L., Golub, T., Mesirov, J. P. et al. (2010), 'Integrated genomic analysis identifies clinically relevant subtypes of glioblastoma characterized by abnormalities in pdgfra, idh1, egfr, and nf1', *Cancer cell* **17**(1), 98–110.

Viventi, J., Kim, D.-H., Vigeland, L., Frechette, E. S., Blanco, J. A., Kim, Y.-S., Avrin, A. E., Tiruvadi, V. R., Hwang, S.-W., Vanleer, A. C. et al. (2011), 'Flexible, foldable, actively multiplexed, high-density electrode array for mapping brain activity in vivo', *Nature neuroscience* **14**(12), 1599.

Weng, H.-R. and Schouenborg, J. (1996), 'Cutaneous inhibitory receptive fields of withdrawal reflexes in the decerebrate spinal rat.', *The Journal of physiology* **493**(1), 253–265.

Zampieri, N., Jessell, T. M. and Murray, A. J. (2014), 'Mapping sensory circuits by anterograde transsynaptic transfer of recombinant rabies virus', *Neuron* **81**(4), 766–778.